



HAL
open science

Rapid estimation of the fatigue limit of Smart Polymer-Matrix Composites (PMC) using the self-heating tests

J. Najd, W. Harizi, Z. Aboura, E. Zappino, E. Carrera

► **To cite this version:**

J. Najd, W. Harizi, Z. Aboura, E. Zappino, E. Carrera. Rapid estimation of the fatigue limit of Smart Polymer-Matrix Composites (PMC) using the self-heating tests. *Composite Structures*, 2022, pp.115039. 10.1016/j.compstruct.2021.115039 . hal-03463978

HAL Id: hal-03463978

<https://hal.science/hal-03463978>

Submitted on 8 Jan 2024

HAL is a multi-disciplinary open access archive for the deposit and dissemination of scientific research documents, whether they are published or not. The documents may come from teaching and research institutions in France or abroad, or from public or private research centers.

L'archive ouverte pluridisciplinaire **HAL**, est destinée au dépôt et à la diffusion de documents scientifiques de niveau recherche, publiés ou non, émanant des établissements d'enseignement et de recherche français ou étrangers, des laboratoires publics ou privés.



Distributed under a Creative Commons Attribution - NonCommercial 4.0 International License

Rapid estimation of the fatigue limit of Smart Polymer-Matrix Composites (PMC) using the self-heating tests.

J. Najd^{1,2)}, W. Harizi^{1*)}, Z. Aboura¹⁾, E. Zappino²⁾, E. Carrera²⁾

*¹⁾ Université de technologie de Compiègne, Roberval (Mechanics, energy and electricity),
Centre de recherche Royallieu - CS 60 319 - 60 203 Compiègne Cedex - France.*

*²⁾ Mul² Group, Department of Mechanical and Aerospace Engineering, Politecnico di Torino,
Corso Duca degli Abruzzi 24, 10129 Torino, Italy.*

**⁾ Corresponding author: walid.harizi@utc.fr*

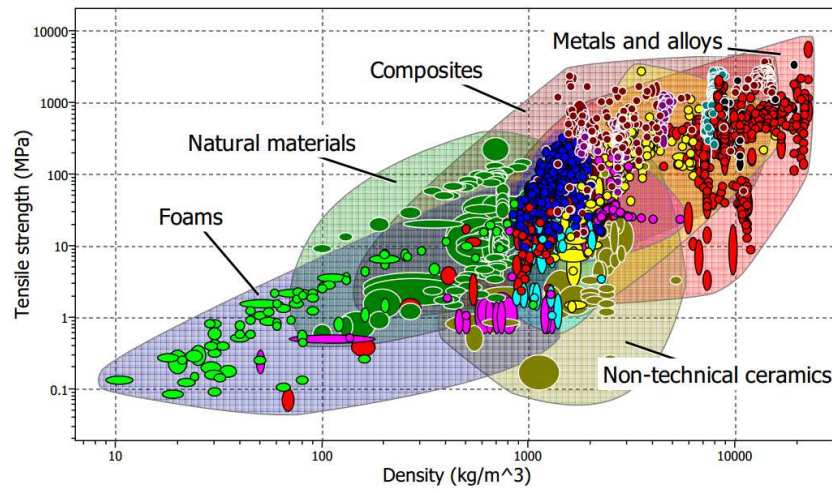
Abstract

Given it is usually highly problematic and time-consuming to evaluate the real in-situ damage and fatigue limit of the polymer-matrix composite (PMC) materials, this study investigates the electrical capacitance variation of polyvinylidene difluoride (PVDF) piezopolymer transducer embedded within PMC specimens made with a polyester resin reinforced by 2/2 twill glass fabrics and submitted to the self-heating tests. During the successive cyclic loadings, the non-intrusiveness of the PVDF sensors was ensured as well as the conformity of the fatigue limit estimated using both stabilized temperature and capacitance measurements. Novel damage estimation curves were proposed based on different temperature and capacitance variables. Thereby, the originality of this study lies in the assessment of the fatigue limit and damage quantification of PMC materials using two physical magnitudes: electrical capacitance and temperature variations. These two quantities provide a fairly fast estimation of the fatigue limit with a slight percentage difference of 9%.

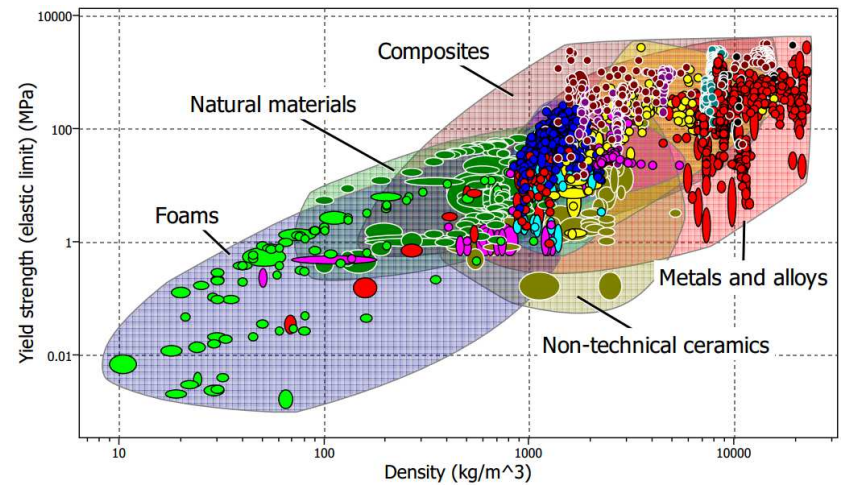
Keywords: Polymer-matrix composites (PMCs); Piezopolymer transducer; Polyvinylidene difluoride (PVDF); Electrical capacitance; Self-heating test; Fatigue limit.

1. Introduction

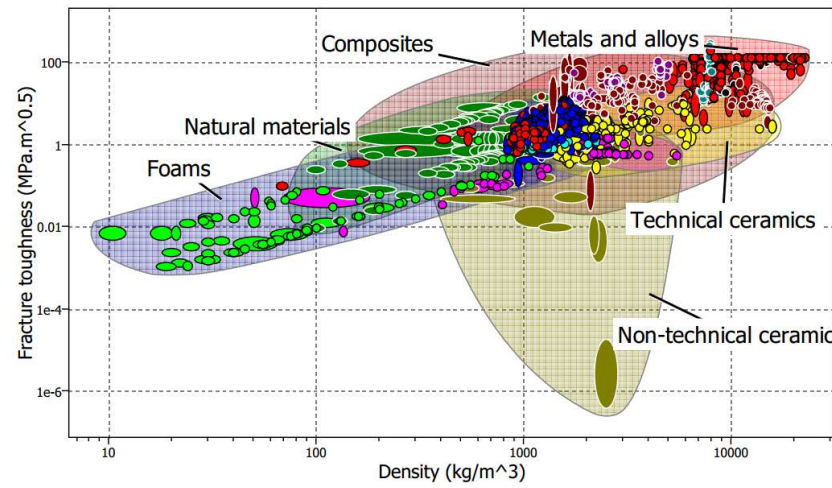
Polymer-matrix composites (PMC) are widely known for their remarkable mechanical properties and their lightweight. They are used in various applications as aerospace, naval, automotive, civil and professional sports applications. The main interests of these materials, in addition to their versatility and relatively low cost, are their combination of corrosion and wear resistance, their thermal and electrical insulation with the glass fibers, electrical conductivity with the carbon fibers [1–7], and most importantly their high specific mechanical properties such as specific tensile strength, specific stiffness and specific impact strength [8]. The specific properties are evaluated by dividing the concerned mechanical property (Young's modulus, Elastic limit, Ultimate Tensile Strength, Fracture toughness,...) by the material density ρ . The graphs of **Figure 1** (using the CES EduPack software) present some specific mechanical properties of the principal families of materials. It is clear that the composite materials family is positioned above (at a higher level) other families regarding the specific tensile strength (**Figure 1a**), specific yield strength (**Figure 1b**), specific fracture toughness (**Figure 1c**), and records the highest specific Young's modulus, right after the technical ceramics (**Figure 1d**). However, despite these very interesting mechanical properties, many structural components made of PMC fail due to the fatigue loadings, even before reaching the yield stress. Furthermore, PMCs are heterogeneous and anisotropic materials, their mechanical properties rely on the manufacturing process and the stacking sequence [9]. These reasons justify the lack of a versatile model able to estimate their fatigue life. This characteristic is conventionally estimated by the S-N or Wöhler curve. To do this, many specimens are tested under cyclic loading with the same mean stress value until failure, and the number of cycles N is registered for each corresponding mean stress. The test is repeated for different stress values, each one several times for repeatability purposes. The construction of the S-N curve is extremely time and energy-consuming as some specimens might endure up to weeks without failure, especially at small stress values.



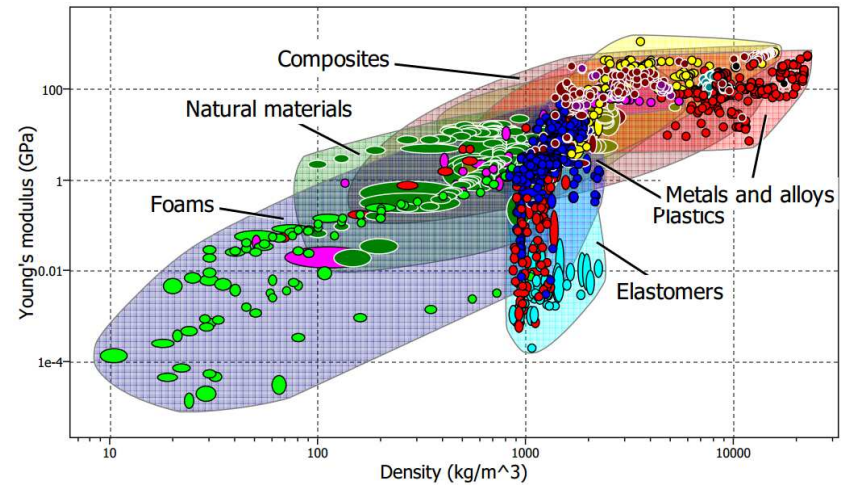
(a)



(b)



(c)



(d)

Figure 1: Mechanical properties of materials as a function of their densities (CES EduPack)

Also, a great number of specimens is needed in order to construct a reliable S-N curve (around 20 specimens [10]), which is a waste of materials and resources. Due to the previously mentioned drawbacks, many researchers worked on finding alternative, faster and less complicated ways to evaluate the fatigue limit. Researchers such as *Locati* [11,12] and *Prot* [13,14] studied the energy dissipation until *Catalbiano et al.* [15] followed by *Risitano and La Rosa* [16] suggested observing the material's surface during cyclic loading by a thermographic camera to investigate the energy dissipation. This method has been updated and used ever since and has proven its reliability to estimate the fatigue limit of conventional and isotropic materials rapidly. It was applied first on the stainless steel and metal alloys using the self-heating phenomenon, then it was used for other materials, like thermosetting polymers, ceramic-matrix composites and especially for some thermoplastic composites due to the vast growth of their application and usage as structural materials [17–28]. However, thermoplastic composites are still considered a challenge due to their high viscoelastic properties that can cause a change in the mechanical behavior of the structure, which stands in the way of obtaining an accurate prediction model [29]. In the proposed self-heating tests, the specimen undergoes a cyclic loading. Nevertheless, unlike in the normal fatigue tests where a single stress amplitude is maintained throughout the test, a successive series of cyclic loadings (loading blocks) of different fixed average stress increments are applied on a sample until failure, maintaining the same stress ratio and frequency in every loading block. The cyclic loading in each block induces heating of the material that stabilizes during a certain number of cycles of each block. This heat is dissipated from the surface of the specimen. At the end of each block, the sample is unloaded and cooled until it reaches its original temperature before the next loading block is started. The fatigue limit is the intersection of the two linear asymptotes noticed in the exponential trend of the variation of the stabilized temperature versus the maximum or average stress variation.

However, infrared thermography (IRT), allowing the measurement of the dissipated temperature of the loaded structure during the self-heating test, is a surface technique and the used IR camera must be placed at a distance in front of the loaded structure to record the thermic scene. This might not be possible on some operating systems and can generate some disturbances. Additionally, an obscuring insulator curtain must be used to isolate the thermic scene and to avoid external radiation disturbances that can alter the temperature measurement [30,31]. Due to these reasons, many studies have investigated alternative ways to assess the fatigue limit and damage of materials. Some studies used the electrical resistance response of carbon fiber-reinforced plastic (CFRP) composites under cyclic tests as an indicator for health

monitoring purposes [7,32–34]. In the reference [35], the authors used the resistance variation of CFRP under self-heating tests to estimate the fatigue limit of the material, while [36] studied integrating carbon fiber armatures inside a glass fabric specimen to detect the matrix cracking of GFRP (glass fiber-reinforced plastic) composite. As the piezoceramic transducers are brittle and present a low damage tolerance, the piezoelectric ones based on thermoplastic polymers such as polyvinylidene difluoride (PVDF) exhibit very high ductility which is added to their recyclability [37,38].

The originality of this paper lies in the use of the capacitance measurements of an embedded thermoplastic piezoelectric transducer within 2/2 twill glass-fiber-reinforced polymer-matrix composites submitted in self-heating tests for rapid estimation of their fatigue limit. After presenting the studied material and the experimental procedures used during the self-heating tests, the results will be presented and discussed with a comparison of the two values of the fatigue limit obtained using temperature and capacitance variation.

2. PMC plates and experimental approaches

2.1. Materials and manufacturing process monitoring of the PMC plates

The composite materials used in this study were manufactured using the Liquid Resin Infusion process (LRI) as described in [39]. Twenty-two plies of 2/2 twill glass fabric (from **Gazechim Composites - France**) were used, each ply with dimensions of 320*300 mm², a surface mass of 280 g/m² and 0.2 mm thickness. These fabrics were associated with 900 g of a thermoset unsaturated polyester resin (**Norester 822 Infusion, Nord Composites**) mixed with Methyl Ethyl Ketone Peroxide (MEKP) hardener (**Ketanolox B180 – C.O.I.M s.p.a**) with 1% concentration (1ml hardener per 100g polyester resin). The embedded thermoplastic piezoelectric transducers are PVDF (**TE Connectivity**). Four transducers of 25 mm in diameter were cut from a bigger sheet (279.4*203.2 mm²) using manual stamping cutting tools. These transducers were positioned above the first half of the plies and connected via thin tinned copper wires of 210 µm diameter after placing the first 11 plies on a glass table pre-coated with a mold release (**Figure 2**). Then, the rest of the plies were stacked above, obtaining a symmetrical and balanced stack. The supplementary materials (peel ply, perforated film, infusion mesh, etc.) were added to facilitate the impregnation process and the plate unmolding after consolidation. The resin feeding system was placed and the vacuum bag was applied (**Figure 3a**). Firstly, the vacuum was fixed to -0.95 bar to compress the dry plies and evacuate the air inside the vacuum bag. After mixing the resin with the hardener and degassing the container for 4 minutes under a vacuum of -0.4 bar, the plate was ready for its infusion phase.

The time between the mixing and the injection phase was 7 min. Before impregnation started, the vacuum of the plate was maintained at -0.8 bar by opening the tap that connects the outlet pipe to the vacuum chamber. Afterward, the inlet tap was opened, allowing the resin to flow into the plate due to the vacuum created at the outlet. During the injection phase, 5 distinct positions of the resin front were recorded (**Figure 3b**). The electrical capacitance variation throughout the impregnation and curing phases was monitored by connecting the copper wires (connected with the PVDF transducers) to an LRC bridge (model HM8118, **Rohde & Schwarz**) with the aid of a 4-channel multiplexer. The five distinct positions of resin during the impregnation phase were spotted in **Figure 3b**.

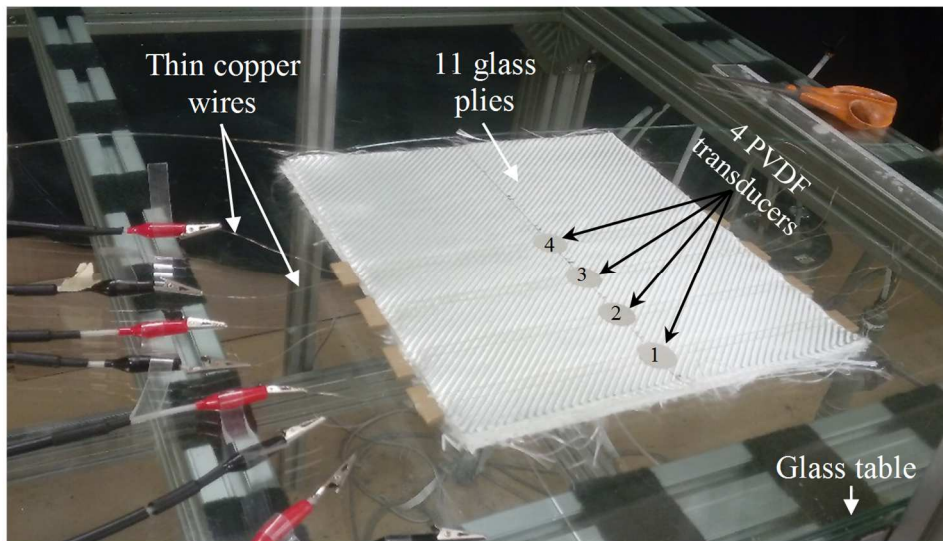
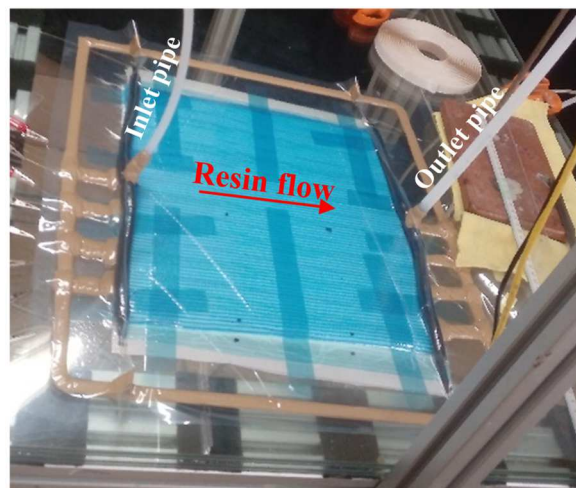


Figure 2: The first half of the glass stacking and positioning of the PVDF transducers



(a)

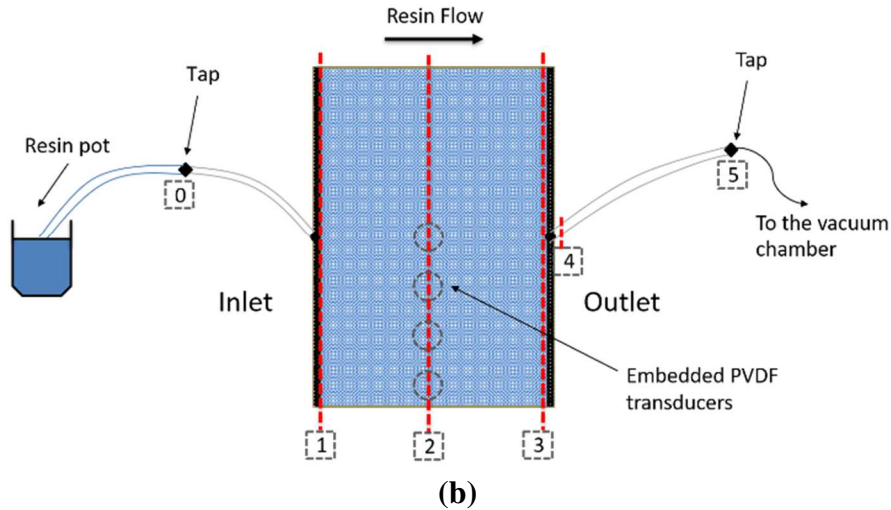


Figure 3: (a) Preparation of the LRI process: vacuum bag and embedded PVDF transducers; (b) Schematization of the five controlled positions during the resin injection.

The electrical capacitance variations of the three transducers 2, 3 and 4 were plotted in **Figure 4** during the injection phase. The electrical capacitance of transducer 1 was not plotted with the others as it could be affected by the edge effect. The electrical capacitance curves show that the embedded transducers react to the resin flow at these five different positions (1 to 5): The capacitance increases as the thermosetting resin is flowing through the dry glass stacking until the resin reaches the PVDF transducers, as when the resin is flowing, it inflates the vacuum bag, causing the increase of the capacitance (from position 1 to 2). After that, when the resin covers the PVDF transducers completely, hydrostatic pressure is generated by the liquid resin and applied on the different sensors until the resin permeates entirely the glass fiber reinforcement (position 3), this behavior causes the drop of the electrical capacitance until it stabilizes (between position 3 and 4). Position 5 refers to the instant when both inlet and outlet pipes are closed simultaneously. When the taps are closed (position 5), there is a slight jump of capacitance since the hydrostatic pressure inside the vacuum chamber decreases. Afterward, the curing phase of the thermosetting resin starts taking place. These results are in agreement with the findings of [39].

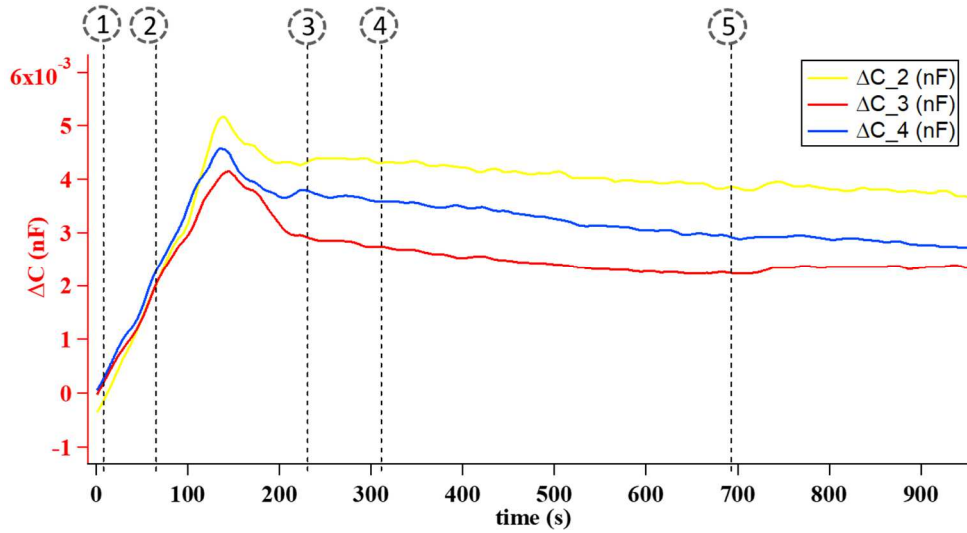


Figure 4: Capacitance variation at the injection phase

The curing process of each PMC plate takes around 7 hours, after which the plate is unmolded. The capacitance variations of the three transducers 2, 3 and 4 were plotted throughout the infusion process until the plate was consolidated (**Figure 5**). Based on **Figure 5**, it is clear that the electrical capacitance variation of the three transducers has the same evolution, increasing at the mid of the process (at around 3 hrs. 20 min) due to the exothermal peak of the crosslinking reaction of the thermosetting resin (the vitrification phase according to [39]). This behavior presumes that resin hardening is homogeneous at the different positions of the embedded transducers.

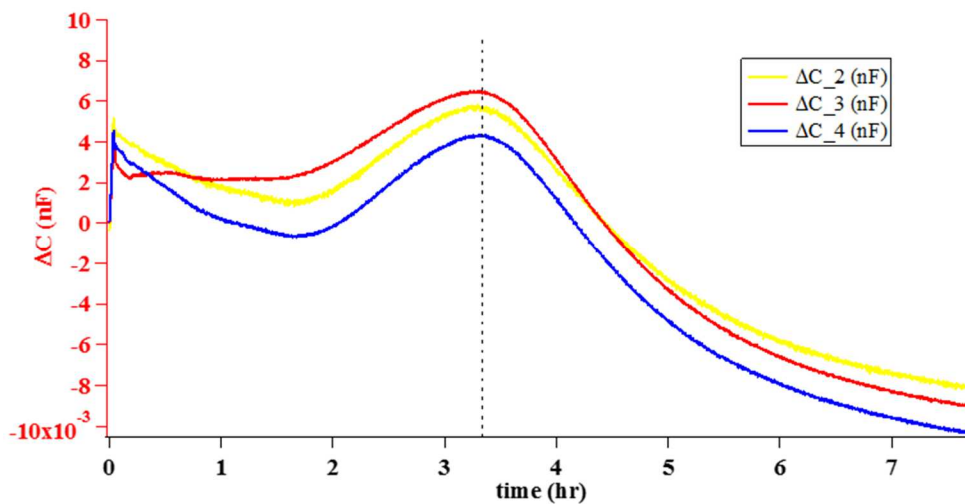


Figure 5: Capacitance variation of the three embedded PVDF transducers 2, 3 and 4 in the same PMC plate

Every time, after unmolding the consolidated PMC plate, the tensile specimens were cut according to the pre-determined dimensions $300 \times 40 \times 5 \text{ mm}^3$ (**Figure 6**), obtaining, for each

PMC plate, three pristine specimens (without PVDF transducer) and four smart ones with integrated PVDF. Four heels ($40 \times 40 \times 2.3 \text{ mm}^3$) were cut and glued to each tensile specimen using a structural adhesive (**Araldite® 2015 A/B**). The obtained samples were then painted black on one side to increase their emissivity during the self-heating tests.

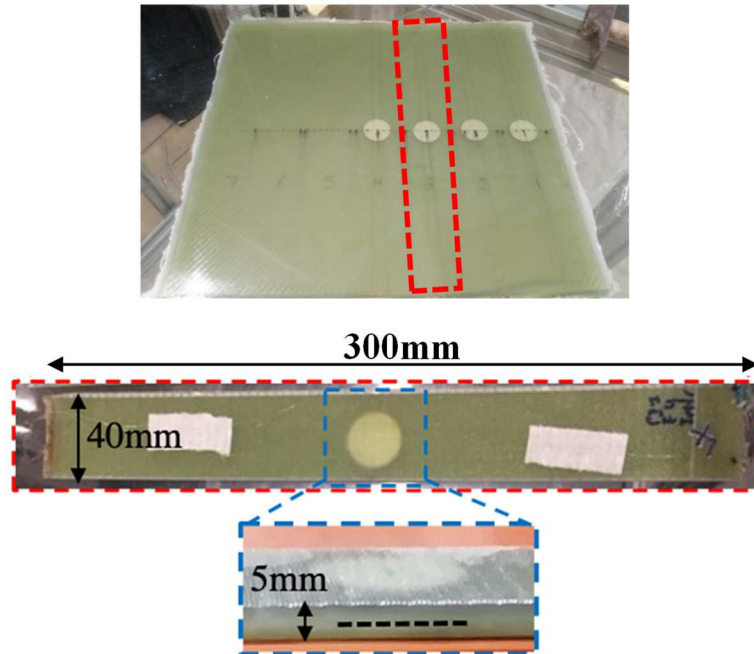


Figure 6: Example of a consolidated PMC plate integrating 4 PVDF transducers after the infusion process, and the exact dimensions of the tensile specimens.

2.2. Experimental approaches

2.2.1. Preliminary study: Heating tests

Heating tests were conducted using an industrial oven (model XL2520, **FRANCE ETUVES**) to evaluate the temperature effect on the electrical capacitance variation. Each thermal test consists in applying on a PMC specimen, integrating a PVDF transducer, a heating ramp with a speed of $0.15 \text{ }^\circ\text{C}/\text{min}$ from an initial temperature of $23 \text{ }^\circ\text{C}$. Once the oven temperature reaches $24 \text{ }^\circ\text{C}$, this temperature is kept constant for 30 minutes. After this, the same PMC specimen is cooled outside the oven until it returns to its initial temperature. Afterward, it will be heated again with the same heating rate until a new stabilized temperature. A total of 5 stabilized oven temperatures were set: 24, 25, 26, 27 and $28 \text{ }^\circ\text{C}$. The maintenance at each stabilized temperature is always 30 minutes. Several PMC samples were tested during this preliminary testing campaign. Every time, two thermocouples (TC1 and TC2 from **TC S.A. France**) were glued on the two surfaces of each PMC sample in order to determine in real-time its true temperature on its two upper and lower faces, respectively. These two thermocouples are positioned in the

center of the PMC specimen, just above and below the PVDF sensor embedded into the core. It should be noted that during each heating test the electrical capacitance measurement of the PVDF transducer was monitored and recorded in real-time by connecting its two copper wires to the LRC bridge. The same LCR bridge (model HM8118, capacitance resolution of 0.01pF, from **Rohde & Schwarz**) is used to record the real-time variations of the in-situ PVDF capacitances during the manufacturing, heating and self-heating experimental campaigns. As it is necessary to apply an AC voltage to the transducer in order to measure its electrical impedance and then extract the electrical capacitance from this measurement, the settings for this sinusoidal voltage are a frequency of 1 kHz and an amplitude of 1 Volt.

2.2.2. *Self-heating tests*

The tests were conducted on the servo-hydraulic fatigue testing machine Instron 1343 with a load cell of 250 kN. The used experimental device (**Figure 7**) consists of the LRC bridge for capacitance measurement, IRT camera and an extensometer. The electrical capacitance was measured with a sampling rate of 1 Hz and its variation was calculated as $\Delta C(t) = C(t) - C(0)$ where $C(t)$ and $C(0)$ are the instantaneous and the initial capacitance values, respectively. The IRT camera (**FLIR** A320 with a pixel resolution of 640(H) × 480(V) and thermal sensitivity of 0.05 °C) was placed at 85 cm from the PMC specimen and the sampling frequency was fixed to 1 Hz (one frame per second). The whole experimental setup was covered with an obscuring black curtain. The instantaneous average temperature variation $\Delta T(t)$ at the center of the specimens was adjusted considering the instantaneous temperature of the hydraulic jaws using Eq. (1) due to their heating during the cyclic loadings [35], where $T(0)$, $T_u(0)$ and $T_l(0)$ are the initial average temperature of the PMC central zone, upper and lower jaw temperatures, respectively. $T(t)$, $T_u(t)$ and $T_l(t)$ are the instantaneous temperatures of the prementioned entities. Eq. (1) allows obtaining the best stabilization of the measured temperature per block. The mechanical loading method implemented in the present study is illustrated in **Figure 8**. It composes of several blocks of cyclic loadings. The values of the parameters of the different loading blocks are summarized in **Table 1**.

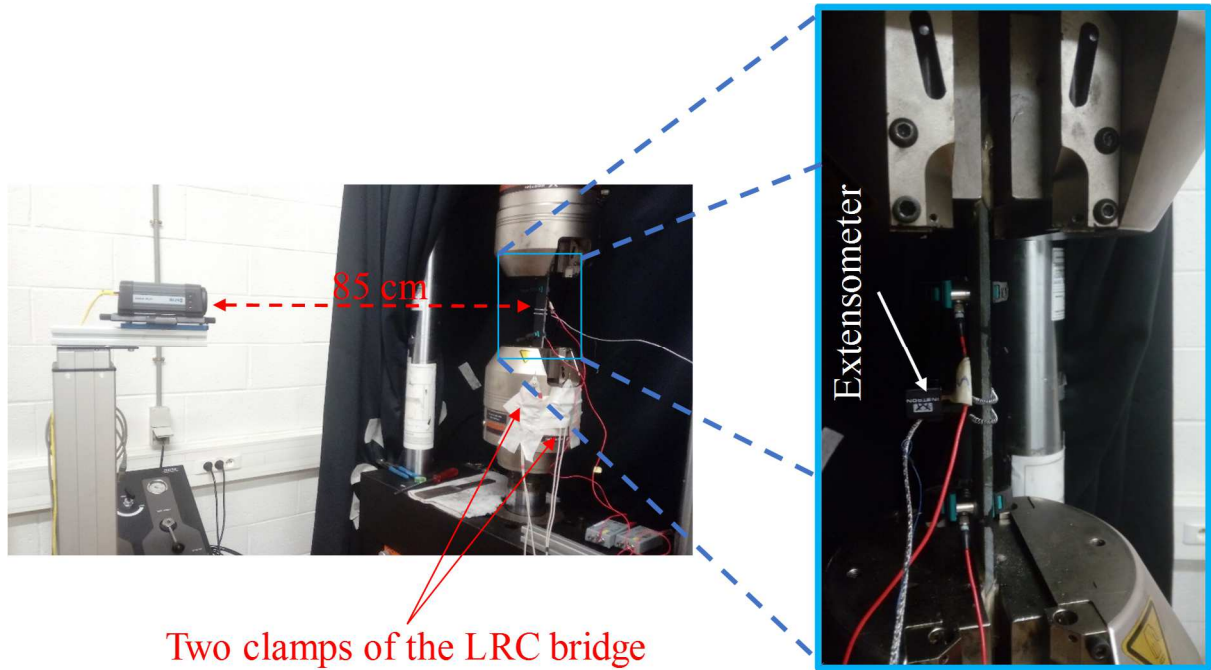


Figure 7: The experimental self-heating device

$$\Delta T(t) = T(t) - T(0) - \frac{T_u(t) + T_l(t)}{2} + \frac{T_u(0) + T_l(0)}{2} \quad [^{\circ}\text{C}] \quad (1)$$

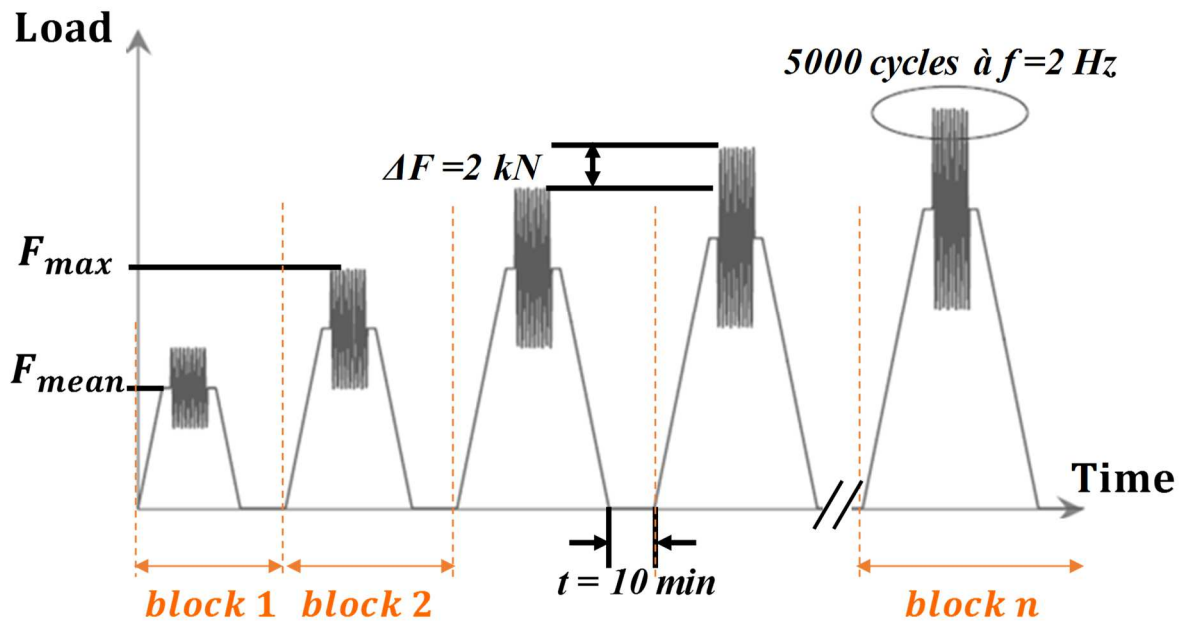


Figure 8: Mechanical loading profile used in the self-heating tests

The cyclic tension-tension loading in the self-heating tests starts from a maximum load of 10 kN (i.e., 50MPa, much lower than the Yield limit) and increases corresponding to 10 MPa incrementation at every block until the failure of the specimen. At the beginning of each block,

the specimen is loaded at a cross-head speed of 2 mm/min until reaching the mean load (F_{mean}). Then, 5000 cycles are applied with a frequency of 2 Hz and load ratio ($R = F_{min}/F_{max}$) of 0.1. During this step, the stabilized temperature and stabilized capacitance are monitored by the IRT camera and LRC bridge, respectively. At the end of the block, the specimen is unloaded at the same cross-head speed (2 mm/min) and maintained unloaded for 10 minutes to cool and regain its initial temperature. Afterward, the load increases again with the next block with the incremental addition of 10 MPa to the prior maximum stress (**Figure 8** and **Table 1**). The acquisition of the load versus time is programmed such that we acquire the first 10 cycles, then one cycle every 10 cycles, then one every 100 cycles and finally one every 500 cycles, in order to improve the (load vs. time) curve displaying and to reduce the size of the acquisition file.

Loading block number	F_{mean} (kN)	σ_{max} (MPa)
block 1	5.5	50
block 2	6.6	60
block 3	7.7	70
block 4	8.8	80
⋮	⋮	⋮
⋮	⋮	⋮

Table 1: Loading blocks used in the self-heating tests

3. Results and discussions

3.1. Heating tests

Figure 9 illustrates the typical results obtained in the heating test conducted on a PMC specimen where the stabilized oven temperature was fixed to 26 °C. The stabilized temperature of the PMC material (TC1 and TC2 in **Figure 9**) measured on the two surfaces of the sample by the two thermocouples exceeds the oven temperature by a few tenths of a degree during the 30-minute hold phase. The difference between TC1 and TC2 is evaluated at 0.2 °C from the start of the test to its end, which is due especially to the rather large thickness of the PMC specimens (5 mm) generating a low thermal gradient. The electrical capacitance variation of the core-integrated PVDF transducer follows the thermal variation: a linear ramp at the start of the heating test, and stabilization as soon as the temperature stabilizes. All these findings were revealed on the different smart PMC samples heated to different stabilized oven temperatures.

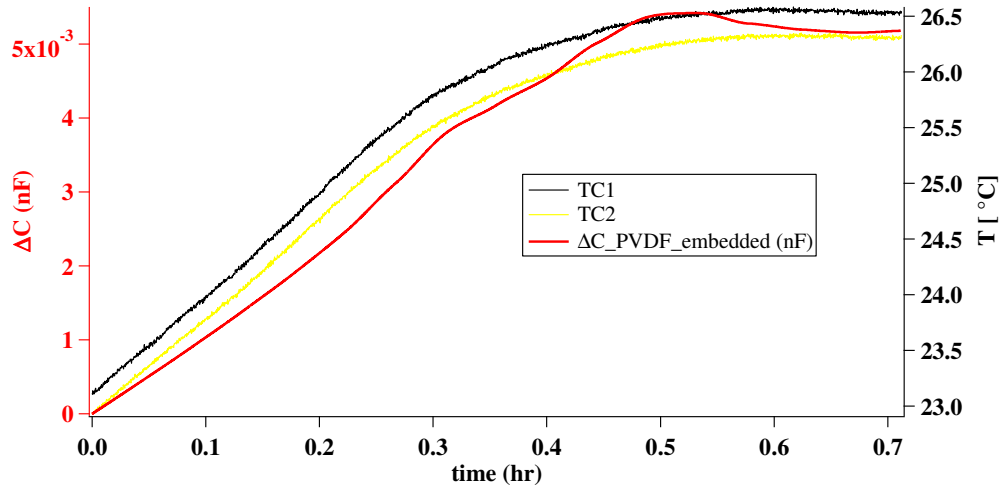


Figure 9: PVDF capacitance and PMC temperature variations during the oven heating test conducted at $0.15\text{ }^{\circ}\text{C}/\text{min}$ and a stabilized temperature of 26°C .

Then, the PVDF capacitance variation was evaluated at each stabilized PMC temperature (the average of TC1 and TC2). The results plotted in **Figure 10** show the linear regression of the electrical magnitude versus the surface temperature of the PMC specimens (thermal magnitude) during the heating tests. Hence, it appears that the electrical capacitance variation measurement of the embedded PVDF can be implemented as a faithful indicator of the temperature variation of the PMC material, and thus can be used to estimate its fatigue limit.

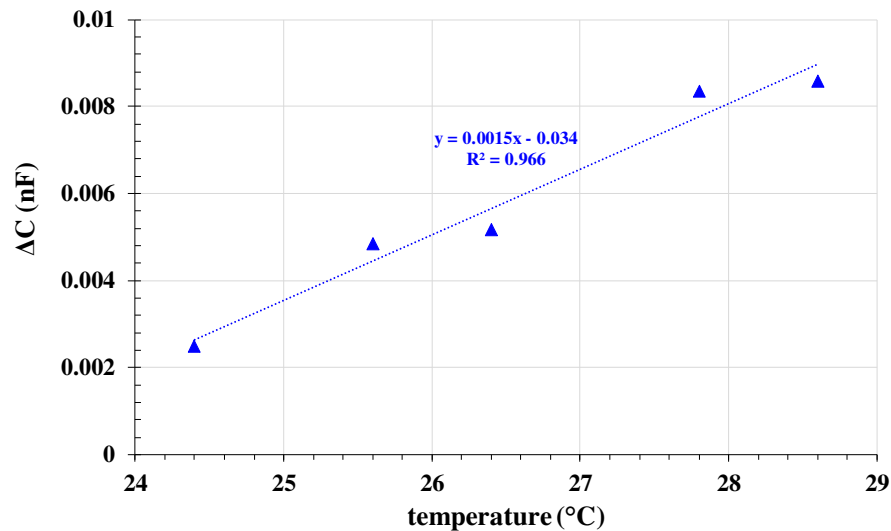


Figure 10: Electrical capacitance variation of PVDF transducer versus the different stabilized sample temperatures during the heating tests.

3.2. Self-heating tests

The (*Stress-Strain*) mechanical behavior recorded during the self-heating tests is illustrated in **Figure 11**. The PMC specimens reach failure at the 13th cyclic loading block and the tensile strain at break measured by the extensometer is evaluated at 0.92%.

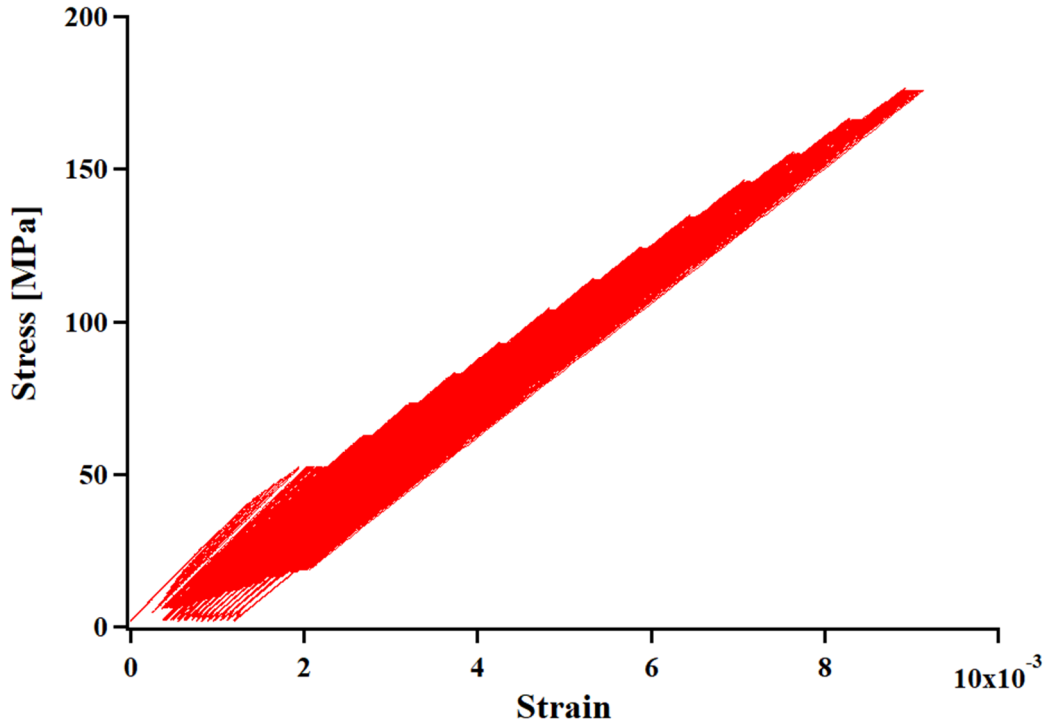


Figure 11: Typical (Stress-Strain) mechanical behaviour recorded during the self-heating tests.

Figure 12 shows the typical capacitance variation ΔC illustrated in a blue continuous line, and the corrected temperature variation ΔT (using Eq. (1)) illustrated in a red continuous line, during the cyclic mechanical loading illustrated in a continuous grey line, that is carried out on a smart PMC specimen. Similarly, **Figure 13** shows the corrected temperature variation ΔT illustrated in a continuous red line during the cyclic mechanical loading plotted with a continuous grey line, that is carried out on a pristine specimen. As the temperature measurement is conducted at distance (85 cm), it is recorded throughout the test until the specimen failure. However, the acquisition of the electrical capacitance of the smart PMC specimens stops before the end of the self-heating test, where the capacitance values can increase highly as a result of the failure of the embedded device, either the PVDF transducer or its connecting wires.

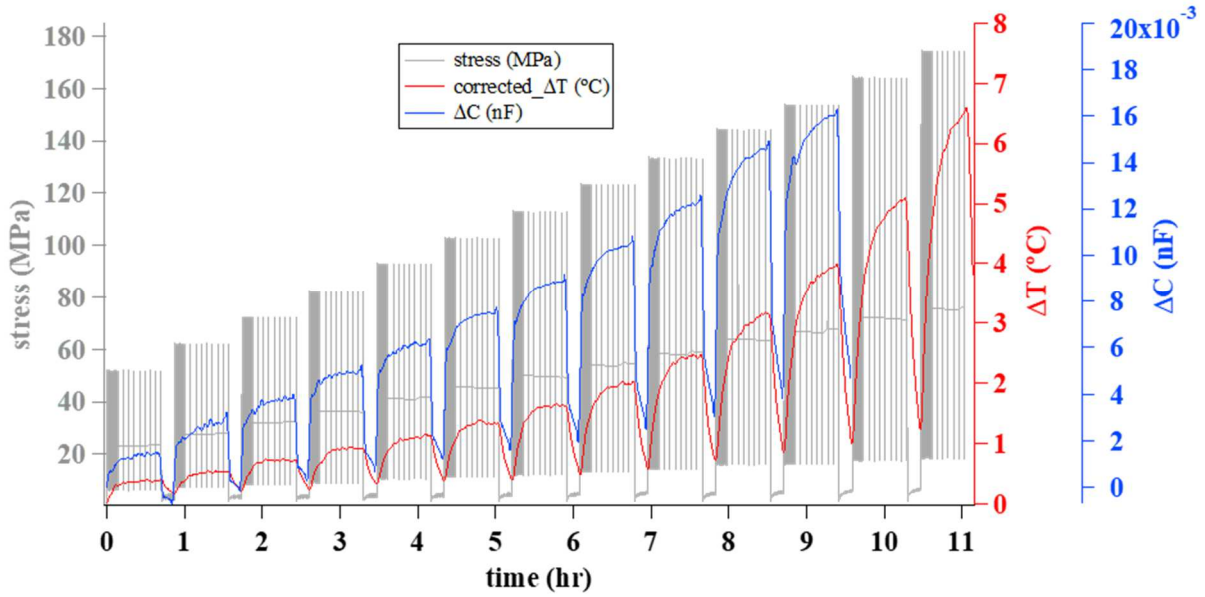


Figure 12: Typical capacitance and temperature variations during the self-heating test conducted on a *smart* PMC specimen

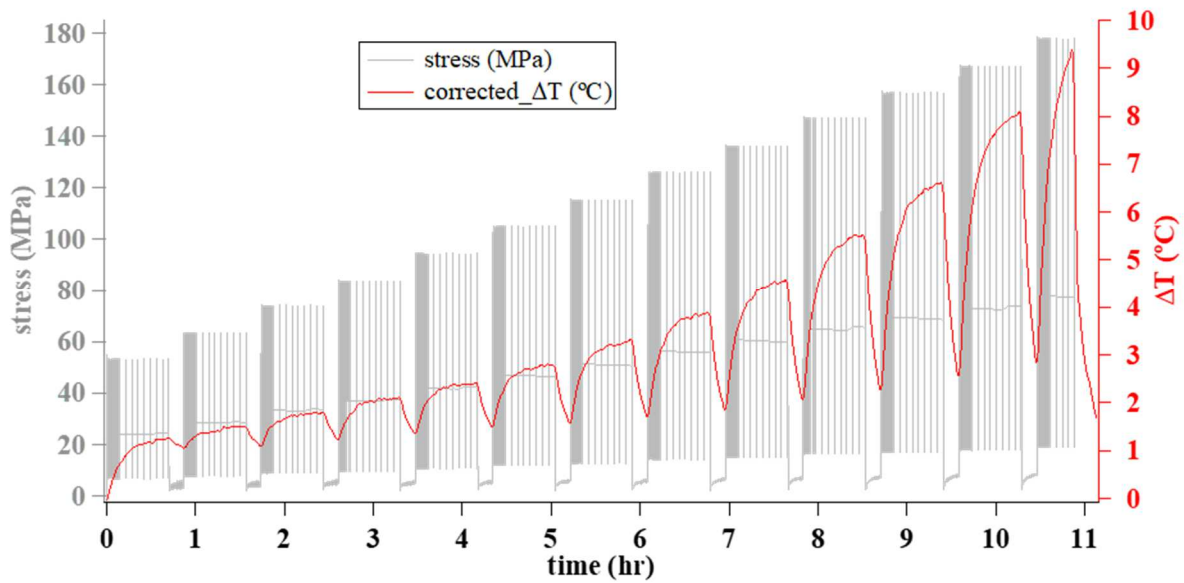


Figure 13: Typical temperature variations during the self-heating test conducted on a *pristine* PMC specimen

During the first mechanical blocks (**Figure 12** and **Figure 13**), the temperature and the capacitance variations return to almost their initial values after unloading the specimen. However, when the damage starts to manifest, the specimens fail to reach their initial temperature and capacitance values while maintained at a zero load for 10 minutes. Likewise, the stabilization of these two entities during the cyclic loading step of each mechanical block is more evident in the first blocks than at the end. This is mainly due to the damage development and accentuation in the material as the loading blocks increase.

Several PMC specimens were tested in the self-heating and the average stabilized temperature variation for the smart and pristine specimens was obtained at each loading block and plotted as a function of the highest stress σ_{max} at the corresponding loading block (**Figure 14** and **Figure 15**). It can be seen that the curve of the stabilized corrected temperature follows two linear regressions. The intersection of the two slopes of the two distinct linear parts in the curve gives a rapid estimation of the fatigue limit of the PMC material. For the smart specimens, this intersection is at **128.2 MPa (Figure 14)** whereas, for the pristine ones, the intersection is at **125.6 MPa (Figure 15)**. The variation between the two estimated limits is just **2.6 MPa**, equivalent to **2%** variation only. This result concludes clearly the non-intrusiveness characteristic of the embedded PVDF transducers within PMC specimens.

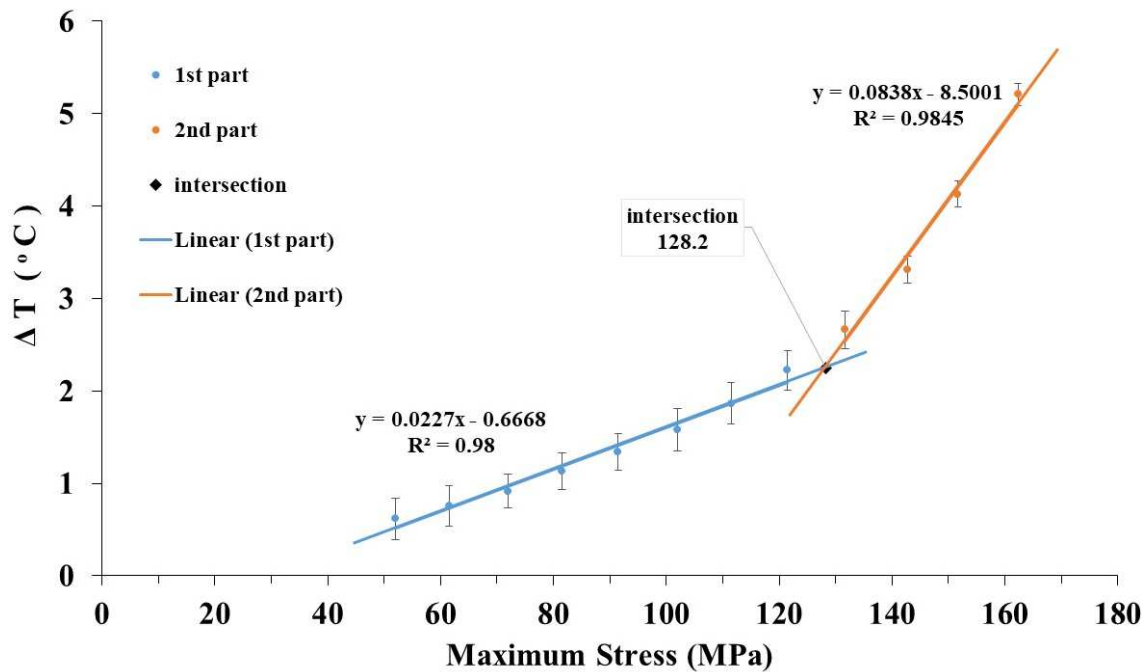


Figure 14: Average stabilized temperatures recorded on the *smart* PMC specimens versus the maximum stresses applied during the self-heating tests.

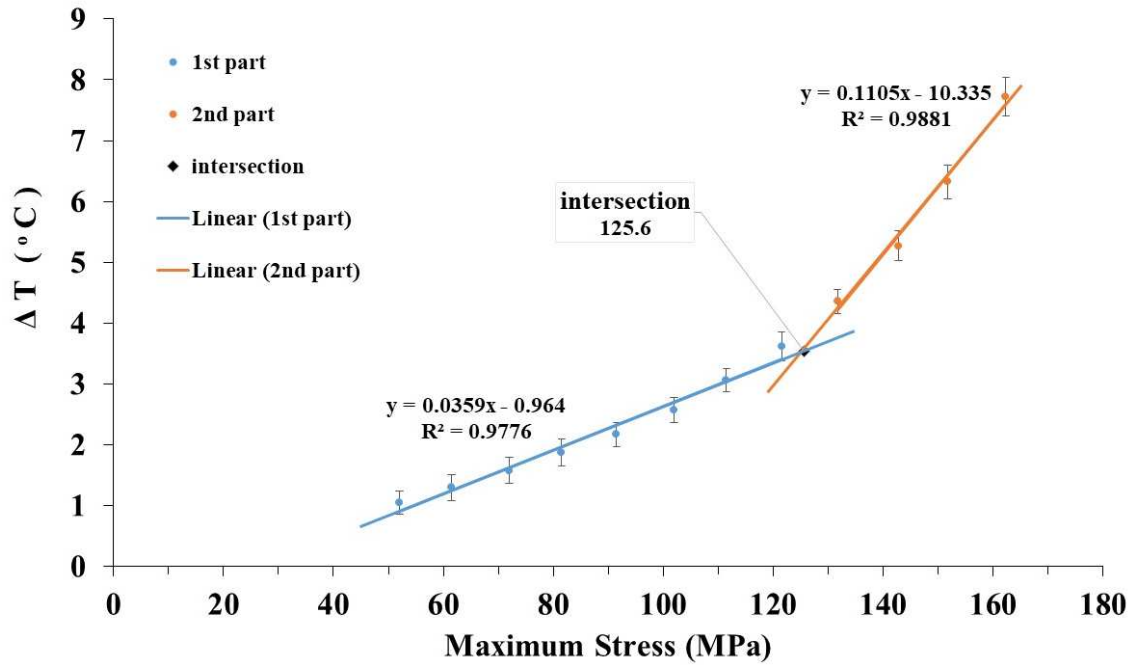


Figure 15: Average stabilized temperatures recorded on the *pristine* PMC samples versus the maximum stresses applied during the self-heating tests.

The average stabilized capacitance variation of the smart specimens was also plotted at each loading block as a function of the highest stress σ_{max} at the corresponding loading block (**Figure 16**). The intersection of the two linear regressions of the two distinct linear parts in the curve gives a rapid estimation of the fatigue limit of the smart PMC material. This intersection is evaluated at **116.67 MPa**. The variation of the estimated fatigue limit by the capacitance and temperature approaches for the smart PMC specimens is **11.53 MPa** which does not exceed the **9%** difference. Nevertheless, it should be noted that the exponential evolution of the (ΔC - σ_{max}) curve is not as obvious as in (ΔT - σ_{max}) one, and hence, the linear trendlines have a small slope variation. This is mainly due to the complex behavior of the electrical capacitance variation, as it is not only linked to the temperature variation but also to the strain of the material in the three principal directions, and to the piezoelectric phenomena at the level of the transducer [37–39].

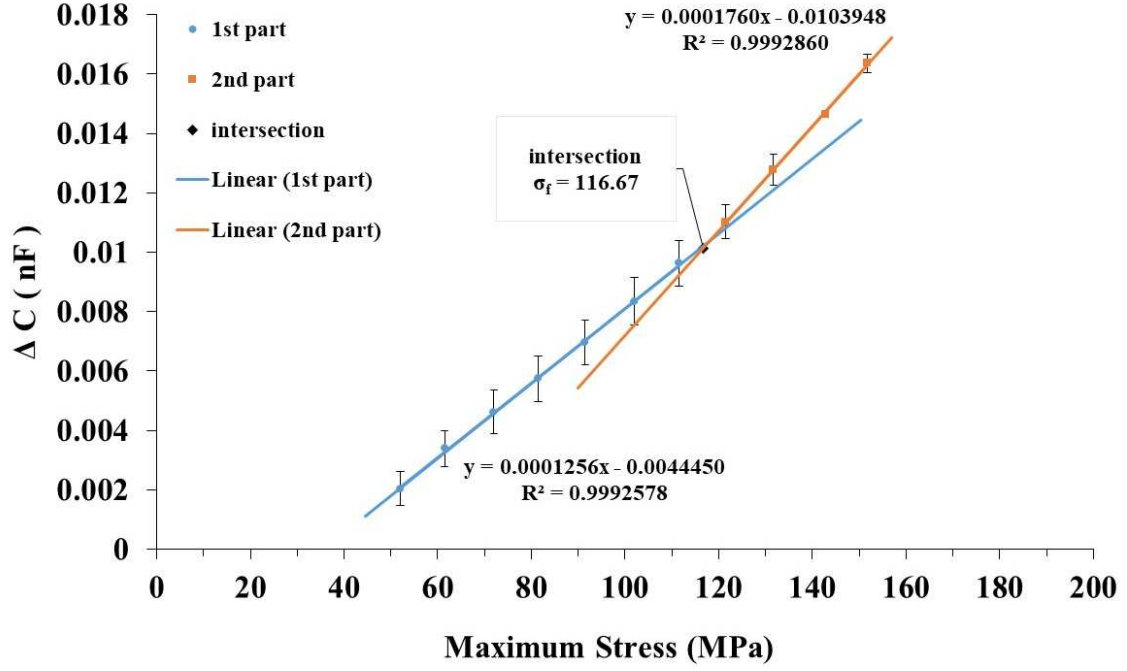


Figure 16: Average stabilized capacitances of the embedded PVDF transducers within smart PMC specimens versus the maximum stresses applied during the self-heating tests.

3.3. Damage quantification

In general, and in a fairly classic way, the damage is quantified using the damage variable calculated based on the rigidity loss of the material $D_E = E_i/E_0$ where E_0 is the initial Young's modulus and E_i is the modulus after each cyclic mechanical loading block. This variable is equal to 1 when the material is purely sound (i.e., $E_i = E_0$) and tends towards 0 when the material is strongly damaged with the mechanical loading increase (E_i becomes weak compared to E_0). In this study, the non-return to the initial temperature combined with the evolution of the temperature decrease rate, both measured at the surface of each PMC specimen, as well as the non-return to the initial electrical capacitance of the core-integrated PVDF transducer are due especially to the development and then the accentuation of the damage within PMC material. Thus, these three characteristics can be used to quantify the damage of the material. For that, three new damage variables ($D_{\Delta T}$, $D_{\Delta C}$ and $D_{\Delta T}$) were defined as the inverses of these three physical magnitudes because the latter increase during the self-heating tests with the increase of the damage inside the material:

- The non-return to the initial corrected temperature variable: $D_{\Delta T} = \frac{1}{(\Delta T_i / \Delta T_0)}$
- The non-return to the initial electrical capacitance variable: $D_{\Delta C} = \frac{1}{(\Delta C_i / \Delta C_0)}$

- The temperature decrease rate variable: $D_{\Delta T} = \frac{1}{(\Delta \dot{T}_i / \Delta \dot{T}_0)}$

For the damage variable $D_{\Delta T}$, the temperature decrease rate is evaluated as being the slope of the $(\Delta T\text{-time})$ curve (**Figure 12**) during the unloading phase of each mechanical block.

These three new damage variables were calculated, plotted and compared with D_E on the same graph in order to evaluate their sensitivities of the damage quantification (**Figure 17**). From the first loading block, the three new variables quantify the damage more than D_E . The $D_{\Delta T}$ and $D_{\Delta C}$ evolve in the same way (the two curves are superimposed) because they are based on the same concept of the non-return to the initial value. On the other hand, it is clear that the $D_{\Delta T}$ variable is the most sensitive because it is calculated over the entire unload step and is not a simple instantaneous value. After the twelfth block, just before the final failure, the classical variable D_E quantifies only 15% in the rigidity loss of the PMC material, while all the new variables exceed a quantification of 75% with a remarkable sensibility of the $D_{\Delta T}$ with a value of 94%. **Figure 17** shows the originality of the use of these new variables in the efficient quantification of the PMC damage.

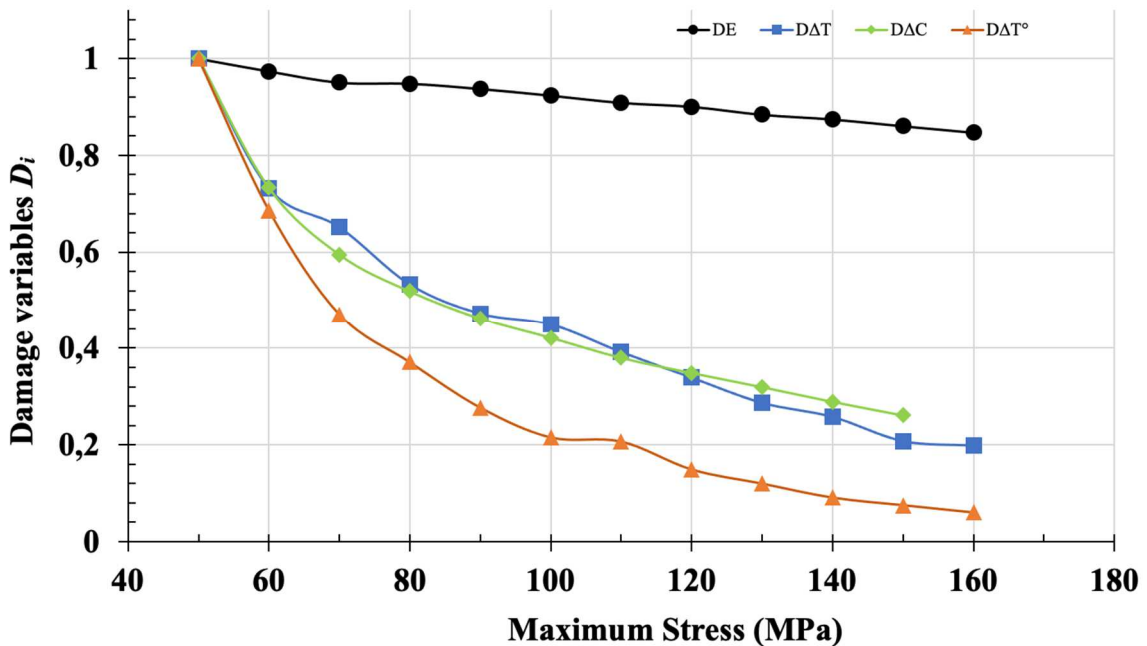


Figure 17: Damage quantification using different new damage variables

4. Conclusions

In this study, pristine (without PVDF transducer) and smart (with PVDF transducer) PMC specimens are made with a polyester resin reinforced by 2/2 twill glass fabrics and submitted to the heating and self-heating tests.

The results of the heating tests reveal that the PVDF electrical capacitance is linear versus the PMC surface temperature variation, making it possible to consider the electrical signature as a faithful indicator of the temperature variation of the PMC material, and thus can be used to estimate its fatigue limit.

In the self-heating tests, the goal was to study the intrusiveness of PVDF transducer integration within PMC material and use its electrical capacitance variation in order to propose a novel approach for the estimation of the fatigue limit of this material. The obtained results prove the non-intrusiveness of the embedded PVDF transducer and support the proposed approach using the electrical capacitance variation to estimate quickly the fatigue limit. However, the exponential evolution of the $(\Delta C-\sigma_{max})$ curve is not as obvious as in the $(\Delta T-\sigma_{max})$ one. This is due to the complex behavior of the electrical capacitance variation, as it is not only linked to the temperature variation but also the strain of the material in the three principal directions, and the piezoelectric phenomena at the level of the transducer.

Finally, the originality of this study lies in two major points:

- The proposal of a new physical magnitude, capacitance measurement during the self-heating tests, for the rapid estimation of the fatigue limit of the PMC materials.
- The use of the electrical capacitance variation to evaluate the health-state of the PMC material by defining three new damage variables more sensible than the classical one using the rigidity loss.

5. Data availability

The raw/processed data required to reproduce these findings cannot be shared at this time as the data also forms part of an ongoing study.

Acknowledgments

The authors would like to thank the Hauts-de-France Region and Politecnico di Torino for the funding of this work as part of the doctoral thesis of Mr. Jamal NAJD. A special thanks goes to the technical staff of the Roberval laboratory of “Université de Technologie de Compiègne” - France.

References

- [1] Jia Z, Li T, Chiang F pen, Wang L. An experimental investigation of the temperature effect on the mechanics of carbon fiber reinforced polymer composites. *Composites Science and Technology* 2018;154:53–63. <https://doi.org/10.1016/j.compscitech.2017.11.015>.

- [2] Saba N, Jawaid M. A review on thermomechanical properties of polymers and fibers reinforced polymer composites. *Journal of Industrial and Engineering Chemistry* 2018;67:1–11. <https://doi.org/10.1016/j.jiec.2018.06.018>.
- [3] Indra Reddy M, Vijaya Kumar Raju P, Bhargava NRMR. Experimental Investigation on the Mechanical and Thermal Properties of Sprouts Center Stem (Asian Palmyra) Fiber Reinforced Polymer Composites. *Materials Today: Proceedings* 2018;5:7808–17. <https://doi.org/https://doi.org/10.1016/j.matpr.2017.11.460>.
- [4] Hamdi K, Aboura Z, Harizi W, Khellil K. Structural health monitoring of carbon fiber reinforced matrix by the resistance variation method. *Journal of Composite Materials* 2020;54:3919–30. <https://doi.org/10.1177/0021998320921476>.
- [5] Martins AT, Aboura Z, Harizi W, Laksimi A, Hamdi K. Structural health monitoring by the piezoresistive response of tufted reinforcements in sandwich composite panels. *Composite Structures* 2019;210:109–17. <https://doi.org/10.1016/j.compstruct.2018.11.032>.
- [6] Martins AT, Aboura Z, Harizi W, Laksimi A, Khellil K. Structural health monitoring for GFRP composite by the piezoresistive response in the tufted reinforcements. *Composite Structures* 2019;209:103–11. <https://doi.org/10.1016/j.compstruct.2018.10.091>.
- [7] Hamdi K, Aboura Z, Harizi W, Khellil K. Improvement of the electrical conductivity of carbon fiber reinforced polymer by incorporation of nanofillers and the resulting thermal and mechanical behavior. *Journal of Composite Materials* 2018;52:1495–503. <https://doi.org/10.1177/0021998317726588>.
- [8] Martins AT, Aboura Z, Harizi W, Laksimi A, Khellil K. Analysis of the impact and compression after impact behavior of tufted laminated composites. *Composite Structures* 2018;184:352–61. <https://doi.org/10.1016/j.compstruct.2017.09.096>.
- [9] Vieira PR, Carvalho EML, Vieira JD, Toledo Filho RD. Experimental fatigue behavior of pultruded glass fibre reinforced polymer composite materials. *Composites Part B: Engineering* 2018;146:69–75. <https://doi.org/10.1016/j.compositesb.2018.03.040>.
- [10] ISO 13003:2003. Fibre-reinforced plastics-Determination of fatigue properties under cyclic loading conditions. 2003.
- [11] Locati L. An aid for the determination of fatigue limit in research and production. *Metall Ital* 1935;27:188–204.
- [12] Locati L. Fatigue and other tests with progressively increasing load. *Eng Dig* 1959;20:337–9.
- [13] Prot M. The determination of the fatigue limit by progressively increased loading. *Misure et Control* 1948;13:301–9.
- [14] Prot M. Fatigue testing under progressive loading. *WADCTR* 1952:53–148.
- [15] Catalbiano T, Geraci A, Orlando M. Analysis of the fatigue strength of specimens by means of the infrared technique. *Il Progettista Industriale* 1984;2:66–9.
- [16] Rosa G la, Risitano A. Thermographic methodology for rapid determination of the fatigue limit of materials and mechanical components. vol. 22. 2000.
- [17] Crupi V, Epasto G, Guglielmino E, Risitano G. Analysis of temperature and fracture surface of AISI4140 steel in very high cycle fatigue regime. *Theoretical and Applied Fracture Mechanics* 2015;80:22–30. <https://doi.org/10.1016/j.tafmec.2015.07.007>.

- [18] Curà F, Curti G, Sesana R. A new iteration method for the thermographic determination of fatigue limit in steels. *International Journal of Fatigue* 2005;27:453–9. <https://doi.org/10.1016/j.ijfatigue.2003.12.009>.
- [19] Plekhov O, NO, SI, PA, & VR. Experimental study of thermodynamic and fatigue properties of submicrocrystalline titanium under high cyclic and gigacyclic fatigue regimes. *Proceedings of the Institution of Mechanical Engineers, Part C: Journal of Mechanical Engineering Science* 2014;229:1271–9.
- [20] Amiri M, Khonsari MM. Rapid determination of fatigue failure based on temperature evolution: Fully reversed bending load. *International Journal of Fatigue* 2010;32:382–9. <https://doi.org/10.1016/j.ijfatigue.2009.07.015>.
- [21] De Finis R, Palumbo D, Ancona F, Galietti U. Fatigue limit evaluation of various martensitic stainless steels with new robust thermographic data analysis. *International Journal of Fatigue* 2015;74:88–96. <https://doi.org/10.1016/j.ijfatigue.2014.12.010>.
- [22] Meneghetti G, Ricotta M, Atzori B. Experimental evaluation of fatigue damage in two-stage loading tests based on the energy dissipation. *Proceedings of the Institution of Mechanical Engineers, Part C: Journal of Mechanical Engineering Science* 2015;229:1280–91. <https://doi.org/10.1177/0954406214559112>.
- [23] Ovalle Rodas C, Zaïri F, Naït-Abdelaziz M. A finite strain thermo-viscoelastic constitutive model to describe the self-heating in elastomeric materials during low-cycle fatigue. *Journal of the Mechanics and Physics of Solids* 2014;64:396–410. <https://doi.org/10.1016/j.jmps.2013.10.010>.
- [24] Le Saux V, Marco Y, Calloch S, Doudard C, Charrier P. An energetic criterion for the fatigue of rubbers: An approach based on a heat build-up protocol and μ -tomography measurements. *Procedia Engineering*, vol. 2, 2010, p. 949–58. <https://doi.org/10.1016/j.proeng.2010.03.103>.
- [25] Gornet L, Wesphal O, Burtin C, Bailleul JL, Rozycki P, Stainier L. Rapid determination of the high cycle fatigue limit curve of carbon fiber epoxy matrix composite laminates by thermography methodology: Tests and Finite Element simulations. *Procedia Engineering*, vol. 66, Elsevier Ltd; 2013, p. 697–704. <https://doi.org/10.1016/j.proeng.2013.12.123>.
- [26] Vergani L, Colombo C, Libonati F. A review of thermographic techniques for damage investigation in composites. *Frattura Ed Integrità Strutturale* 2014;8:1–12. <https://doi.org/10.3221/IGF-ESIS.27.01>.
- [27] Kordatos EZ, Dassios KG, Aggelis DG, Matikas TE. Rapid evaluation of the fatigue limit in composites using infrared lock-in thermography and acoustic emission. *Mechanics Research Communications* 2013;54:14–20. <https://doi.org/10.1016/j.mechrescom.2013.09.005>.
- [28] Muller L, Roche JM, Hurmane A, Pacou D, Bonnand V, Peyrac C, et al. Experimental monitoring of the self-heating properties of thermoplastic composite materials. *Procedia Engineering*, vol. 213, Elsevier Ltd; 2018, p. 183–91. <https://doi.org/10.1016/j.proeng.2018.02.020>.
- [29] Mortazavian S, Fatemi A, Mellott SR, Khosrovaneh A. Effect of cycling frequency and self-heating on fatigue behavior of reinforced and unreinforced thermoplastic polymers. *Polymer Engineering and Science* 2015;55:2355–67. <https://doi.org/10.1002/pen.24124>.
- [30] Harizi W, Chaki S, Bourse G, Ourak M. Mechanical damage assessment of Glass Fiber-Reinforced Polymer composites using passive infrared thermography. *Composites Part B: Engineering* 2014;59:74–9. <https://doi.org/10.1016/j.compositesb.2013.11.021>.

- [31] Harizi W, Chaki S, Bourse G, Ourak M. Mechanical damage assessment of Polymer-Matrix Composites using active infrared thermography. *Composites Part B: Engineering* 2014;66:204–9. <https://doi.org/10.1016/j.compositesb.2014.05.017>.
- [32] Todoroki A, Haruyama D, Mizutani Y, Suzuki Y, Yasuoka T. Electrical Resistance Change of Carbon/Epoxy Composite Laminates under Cyclic Loading under Damage Initiation Limit. *Open Journal of Composite Materials* 2014;04:22–31. <https://doi.org/10.4236/ojcm.2014.41003>.
- [33] Vavouliotis AI, Kostopoulos V. On the use of electrical conductivity for the assessment of damage in carbon nanotubes enhanced aerospace composites. *Solid Mechanics and Its Applications* 2013;188:21–55. https://doi.org/10.1007/978-94-007-4246-8_2.
- [34] Chung DDL. Processing-structure-property relationships of continuous carbon fiber polymer-matrix composites. *Materials Science and Engineering R: Reports* 2017;113:1–29. <https://doi.org/10.1016/j.mser.2017.01.002>.
- [35] Harizi W, Azzouz R, Martins AT, Hamdi K, Aboura Z, Khellil K. Electrical resistance variation during tensile and self-heating tests conducted on thermoplastic polymer-matrix composites. *Composite Structures* 2019;224. <https://doi.org/10.1016/j.compstruct.2019.111001>.
- [36] Buggisch C, Gagani A, Fiedler B. Capacitance measurements on integrated conductors for detection of matrix cracks in GFRP. *Functional Composite Materials* 2021;2. <https://doi.org/10.1186/s42252-020-00013-x>.
- [37] Tuloup C, Harizi W, Aboura Z, Meyer Y. Integration of piezoelectric transducers (PZT and PVDF) within polymer-matrix composites for structural health monitoring applications: new success and challenges. *International Journal of Smart and Nano Materials* 2020. <https://doi.org/10.1080/19475411.2020.1830196>.
- [38] Tuloup C, Harizi W, Aboura Z, Meyer Y. Structural health monitoring of polymer-matrix composite using embedded piezoelectric ceramic transducers during several four-points bending tests. *Smart Materials and Structures* 2020;29:125011. <https://doi.org/10.1088/1361-665X/abbc59>.
- [39] Tuloup C, Harizi W, Aboura Z, Meyer Y, Ade B, Khellil K. Detection of the key steps during Liquid Resin Infusion manufacturing of a polymer-matrix composite using an in-situ piezoelectric sensor. *Materials Today Communications* 2020;24. <https://doi.org/10.1016/j.mtcomm.2020.101077>.